Wind and Structures, *Vol. 29, No. 6 (2019) 441-455*
DOI: https://doi.org/10.12989/was.2019.29.6.441

Vortex induced vibration analysis of a cylinder mounted on a flexible rod

Mehdi Zamanian*[1] and Luigi Garibaldi[2a]

[1]*Department of Mechanical Engineering, Faculty of Engineering, Kharazmi University, P.O. Box 15719-14911, Tehran, Iran*
[2]*Dipartimento di Ingegneria Meccanica e Aerospaziale, Politecnico di Torino, C.so Duca degli Abruzzi, 24, 10129, Torino, Italy*

(Received March 18, 2019, Revised June 17, 2019, Accepted June 28, 2019)

Abstract. In this study, vortex induced vibrations of a cylinder mounted on a flexible rod are analyzed. This simple configuration represents the key element of new conception bladeless wind turbine (Whitlock 2015). In this study the structure oscillations equation coupled to the wake oscillation equation for this configuration are solved using analytical perturbation method, for the first time. An analytical expression that predicts the lock-in phenomena range of wind speed is derived. The discretized equations of motion are also solved using RKF45 numerical method. The equations of motion are discretized by Galerkin method. Free vibration mode shape of the structure taking into account the discontinuity of the cross section are used as comparison function. Numerical results are compared to the analytical results, and they show a satisfying agreement. The effect of system parameters on the oscillations of structure and wake as well as on the lock-in domain are presented. Moreover, it is shown that the values of wind speed triggering the start and the stop of the lock-in phenomenon, for increasing wind speed are different from those values obtained during the reverse process, i.e., when the wind speed decreases.

Keywords: vortex induced vibration; lock-in; van der Pol wake oscillator; circular cylinder; perturbation method

1. Introduction

Boundary layer separation often occurs when fluid is passing over a bluff body. This separation causes a fluid rotation and vortex shedding behind the body. Depending on the value of Reynolds number, the vortex pattern shedding might result periodic. The periodic pattern causes a periodic lift force on the bluff body, which can result in vibrations of the body due to its flexibility or when it is mounted on a flexible support. This type of vibration is usually called vortex induced vibration or VIV (Bearman 1984).

When the vortex shedding frequency approaches the natural frequency of the oscillator, a significant increase in the amplitude of the oscillations of the system (a cylinder in studied case) takes place. This event is called lock-in phenomenon. There are two main differences between linear resonance and lock-in. Unlike linear resonance, lock-in is a nonlinear phenomenon and the vibration of the structure changes itself the vortex shedding. Secondly, lock-in happens over a band of frequencies and does not show a sharp peak in amplitude (Blevins 1990).

Many structures such as long buildings, marine risers, offshores, mooring cables, bridges, nuclear reactors, conductors, cooling stacks and wind turbine blades experience the vortex induced vibration. Lock-in phenomenon is an important factor in their designing, and it may result in serious damage, or even collapse, when it is not taken into account. The collapse of Tacoma Narrows Bridge in the U.S. in 1940 is one of the most known collapses due to VIV in the word (Kim Vandiver *et al*. 2009), (Chaplin *et al*. 2005), (Abdul Nariman 2016), (Wang *et al*. 2016a, b), (Leblond and Hardy 2005), (Sun *et al*. 2013).

In spite of the disadvantage introduced by VIV, its effects may be advantageous in some cases. Recently, the use of VIV for energy harvesting has been considered by researchers. In some of these applications, a configurations with a rectangular beam excited by aerodynamic forces is considered; these forces are applied on a bluff body attached to the extreme of a cantilever beam and the large vibration experienced is then converted to electricity by a piezoelectric layer coated on the flexible beam (Dai *et al.* 2018), (Abdelkefi *et al.* 2013), (Song *et al*. 2015).

VIVACE is the name given to a similar system, proposed by Bernitsas and Raghavan from the University of Michigan, assembled like a rigid cylinder bluff body on a flexible base. In this system, the horizontal hydrokinetic energy of water flow is converted into vertical vibrations of the cylinder. The latter is then converted to electricity through some electric power generators (Bernitsas *et al.* 2008). The idea of bladeless wind turbine as a new application of VIV has been also proposed by a Spanish group (Whitlock 2015). In this project, a cylinder vertically mounted on an elastic rod oscillates due to the interaction between fluid and structure; the latter then generates electricity through an alternator system. Another configuration of bladeless wind turbine has been proposed by Salvador *et al.* (2017). It is an arc-shaped, or disc-shaped, magnet pendulums attached to the end of a cylinder under VIV. The energy of the wind converts to electricity by moving the magnet inside the coil, which behaves as a

*Corresponding author, Associate Professor
E-mail: zamanian@khu.ac.ir; zamaniankhu@gmail.com
[a] Professor
E-mail: luigi.garibaldi@polito.it

ISSN: 1226-6116 (Print), 1598-6225 (Online)

stator on each side of the pendulum generator.

Considering both advantages and disadvantages of VIV, many researches have been developed to model a mathematical formulation for the lift force during VIV on the structure. Most of them are focused on a cylinder mounted on the spring under VIV. If the structure is a flexible cylinder under VIV, then the solution of Navier Stokes equations in presence of moving boundaries is necessary to model the system, and it results quite complex (Chizfahm *et al.* 2018). Therefore, for simplicity, many researchers focused on the semi-empirical model. One of the most accurate models which simulates the dynamic behavior of a cylinder under VIV is in fact the semi-empirical wake model proposed by Skop and Griffin (1973) and Griffin *et al*. (1973). This model, which has been modified by Skop and Balasubramanian (1997), describes the cross-flow fluid force by mean of a van der Pol differential equation. This equation is coupled to the structural motion by a velocity structural term in its right hand side (Skop and Luo 2001). Following this, Facchinetti *et al.* (2004a) showed that the acceleration coupling term introduced in the van der Pol wake oscillator better predicts the system dynamic behavior than velocity and displacement coupling. A modified wake oscillator model has been introduced by Farshidianfar and Zanganeh (2010) to increase the possibility of using wake model for a wider range of mass-damping ratios. Some coefficients for calculating the empirical parameters which have been settled as constants by Facchinetti *et al.* (2004a) have been presented by Wan-hai *et al*. (2010) as variable. A wake oscillator model based on van der Pol model with nonlinear coupling term has been proposed also by Qu and Metrikine (2010). An attempt for improving the Facchinetti *et al*. model has been carried on by Ogink and Metrikine (2010), introducing the frequency dependent coupling. Postnikov et al. proposed two degrees-of-freedom wake oscillator model for describing vortex-induced vibrations of elastically supported cylinders capable of moving both in cross-flow and in-line directions (Postnikov *et al.* 2017). Afterwards, a modification to this model has been investigated by Kurushina and Pavlovskaia (2017).

Another group of researches is also devoted to the use of wake model to simulate the dynamic behavior of continuous system for practical application. The oscillations of flexible slender cables and riser coupled with the Facchinetti *et al*. wake oscillator has been investigated by Violette *et al*. (2007), Facchinetti *et al*. (2004b), Mathelin and de Langre (2005), using the harmonic balance approach. Keber and Wiercigroch (2007) considered the dynamic response of a simply supported offshore riser by introducing the nonlinear geometry terms. They demonstrated that, although the frequency response of the nonlinear system is very close to the linear one, the difference in amplitudes is substantial even for small tensile forces. The vortex induced response of slender cantilever cylindrical beam has been investigated by Leclercq and de Langre (2018). The Strouhal number linked with the vortex shedding frequency, assumed as constant in previous works, has been considered as a function of the Reynolds number for a simply supported flexible cylinder by Gao *et al*. (2018). They solved the equation of motion coupled with van der Pol, taking into account the primary harmonic function and showed that one can obtain more accurate results. An experimental work for vortex-induced vibration of a long flexible cylinder pinned at both sides in uniform cross-flow has been presented by Ji *et al.* (2018). The equations of motion of VIV of a rigid cylindrical bluff body mounted at the end of a flexible slender cantilever beam have been solved numerically by Dai *et al*. (2014). Song *et al*. (2015) and Jia *et al*. (2018) investigated VIV of rigid cylindrical bluff body mounted at the end of a flexible slender cantilever beam by both experimental and numerical method. Chizfahm *et al.* (2018) investigated a numerical solution on the discretized equation by Galerkin method when the cylinder is mounted on a flexible rod. Recently Zhang *et al.* (2019) developed an experimental work to investigate the effect of interference cylinder with different geometry on the VIV of a rigid cylindrical bluff body mounted at the end of a flexible slender cantilever beam.

In this study, vortex induced vibrations of a cylinder mounted on a flexible beam are analyzed. The literature review shows that an analytical study for the vortex induced vibration of this configuration has not been published yet, and here it is presented. In this work the structure oscillations equation coupled to the wake oscillations equation are solved using multiple scale perturbation method, for the first time. An analytical expression that predicts the lock-in phenomenon range of wind speed is derived. The discretized equations of motion are also solved using RKF45 numerical method. Results show a good agreement between numerical and analytical methods, which represents a valuable starting point for theory verification and further work. It must be noted that most of previous works consider the cylinder mounted on a slender rectangular beam and, only Chizfahm *et al.* (2018) considered it mounted on a circular rod. As mentioned before, it represents the key element of new conception bladeless wind turbine (Whitlock 2015). Here, the lift force is evaluated according to van der Pol wake oscillator model improved by Facchinetti *et al*. (2004a), which is more accurate in comparison with the wake oscillator model used by Chizfahm *et al.* (2018). In addition, by applying some assumptions to the model, it represents a multiple scale solution for a vortex induced vibration of a rigid cylinder mounted on flexible spring as was analyzed by harmonic balance in previous work by Facchinetti *et al.* (2004a). The results are compared together and, again, show a good agreement. Here, equations of motion are discretized by Galerkin method using the exact mode shape of free vibration of system i.e. the mode shape considering the non-uniformity of the cross section. The diagrams of steady state amplitude of the structure oscillation and wake oscillation with respect to the wind speed are extracted for different values of system parameters. Moreover, their effects on the lock-in domain are evidenced.

2. Modeling and formulation

The system consists of a cylindrical bluff body mounted

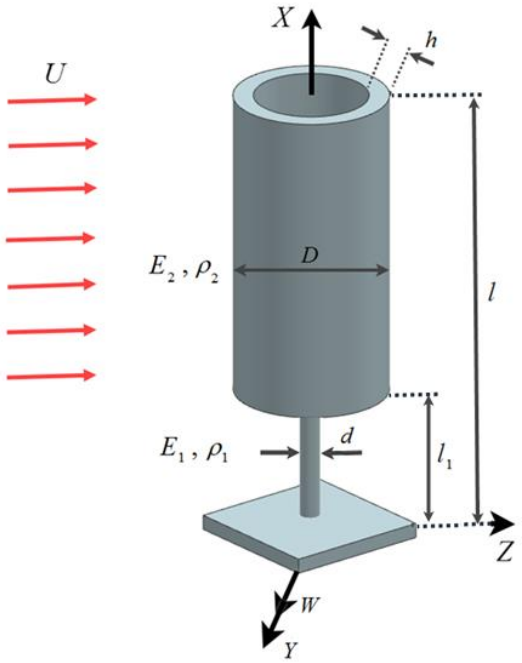

Fig. 1 System configuration subjected to vortex induced vibration

over a flexible rod, such as shown in Fig. 1. The cylinder is subject to the wind flow with $300 < \mathrm{Re} < 1.5\times10^5$ in direction Z, whilst the system vibrates in direction Y due to periodic nature of vortex shedding behind the cylinder. The equation of motion is hence given by

$$E(X)I(X)\frac{\partial^4 W(X,t)}{\partial X^4}+C(X)\frac{\partial W(X,t)}{\partial t}+M(X)\frac{\partial^2 W(X,t)}{\partial t^2}=F(X,t) \quad (1)$$

Where W indicates the transverse deflection of system along direction Y, $M(X)$ indicates the total amount of structure mass and fluid mass per unit length, $E(X)I(X)$ is the bending stiffness, and $C(X)$ is the damping coefficient per unit length, due to wind flow.

$F(X,t)$ is the lift force per unit length, which is related to wake oscillator variable $Q(X,t)$ as below (Facchinetti *et al.* 2004a)

$$\begin{aligned} &F(X,t)=\frac{1}{4}\rho_f U^2 C_{L0} D Q(X,t)\,\mathrm{H}(X-l_1),\\ &\mathrm{H}(X-l_1)=Heaviside(X-l_1)=\begin{cases}0 & X<l_1,\\ 1 & X\ge l_1\end{cases}\end{aligned} \quad (2)$$

where D is the diameter of the cylinder, and l_1 is the length of the rod. ρ_f is the mass per unit volume of the wind, and U is the wind speed. The wake oscillator variable, $Q(X,t)$, is defined as $2C_L(t)/C_{L0}$, where $C_L(t)$ is the time variable lift coefficient, and C_{L0} is the lift coefficient amplitude on a fixed cylindrical structure experiencing vortex shedding, and is equal to 0.3 over a large range of Reynolds number (Facchinetti *et al.* 2004b). The wake oscillator variable is coupled to the structure motion as follows (Facchinetti *et al.* 2004a)

$$\frac{\partial^2 Q(X,t)}{\partial t^2}+\eta(2\pi S_T\frac{U}{D})(Q^2(X,t)-1)\frac{\partial Q(X,t)}{\partial t}+(2\pi S_T\frac{U}{D})^2 Q(X,t)=\frac{G}{D}\frac{\partial^2 W(X,t)}{\partial t^2} \quad (3)$$

where S_T is the Strouhal number which is approximately constant and equal to 0.2 in range $300 < \mathrm{Re} < 1.5\times10^5$. η and G are the damping van der Pol parameter and the coupling coefficient, and are typically equal to 0.3 and 12, respectively (Facchinetti *et al.* 2004a). The functions of $E(X)I(X)$ and $M(X)$ are given as below

$$\begin{aligned} &E(X)I(X)=E_1I_1(1-\mathrm{H}(X-l_1))+E_2I_2\,\mathrm{H}(X-l_1),\\ &m(X)=\rho_1A_1(1-\mathrm{H}(X-l_1))+(\frac{\pi}{4}\rho_f D^2C_M+\rho_2A_2)\,\mathrm{H}(X-l_1),\\ &C(X)=(2\pi S_T\frac{U}{D}\gamma\rho_f D^2)\,\mathrm{H}(X-l_1),\\ &\gamma=\frac{C_D}{4\pi S_T}\end{aligned} \quad (4)$$

where ρ_1 and ρ_2 are the mass density, A_1 and A_2 are the cross sections areas, I_1 and I_2 are the second area moment, and E_1 and E_2 are the elasticity modulus of the rod and cylinder, respectively. In addition C_M is the added mass coefficient due to the fluid, and γ is a stall parameter which is directly related to the mean sectional drag coefficient of the structure C_D. For analytical convenience, the following changes in variables are applied to the equations of motion.

$$w=\frac{W}{D},\quad x=\frac{X}{l},\quad \tau=\frac{t}{T},\quad T=\sqrt{\frac{\rho_1 A_1 l^4}{E_1 I_1}} \tag{5}$$

Where l is the total length of the structure. By applying the above variables changes into Eq. (1) the dimensionless form of motion equations assume the form

$$\begin{aligned}&\bar{E}(x)\bar{I}(x)\frac{\partial^4 w(x,t)}{\partial x^4}+\bar{c}(x)\Omega_f\frac{\partial w(x,t)}{\partial t}+\bar{m}(x)\frac{\partial^2 w(x,\tau)}{\partial \tau^2}=\bar{f}(x)\Omega_f^2 Q,\\&\frac{\partial^2 Q(x,\tau)}{\partial \tau^2}+\eta(Q^2(x,\tau)-1)\frac{\partial Q(x,\tau)}{\partial \tau}+\Omega_f^2 Q(x,\tau)=G\frac{\partial^2 w(x,\tau)}{\partial \tau^2}\end{aligned} \tag{6}$$

where

$$\begin{aligned}&\bar{E}(x)\bar{I}(x)=(1-\mathrm{H}(x-\frac{l_1}{l}))+\frac{E_2 I_2}{E_1 I_1},\\&\bar{m}(x)=(1-\mathrm{H}(x-\frac{l_1}{l}))+\frac{\frac{\pi}{4}\rho_f D^2 C_M+\rho_2 A_2}{\rho_1 A_1}\mathrm{H}(x-\frac{l_1}{l}),\\&\bar{c}(x)=\frac{\gamma\rho_f D^2}{\rho_1 A_1}\mathrm{H}(x-\frac{l_1}{l}),\\&\bar{f}(x)=\frac{\rho_f C_{L0} D^2}{16\pi^2\rho_1 A_1 S_T^2}\mathrm{H}(x-\frac{l_1}{l})\\&\Omega_f=\frac{2\pi S_T U T}{D}\end{aligned} \tag{7}$$

3. Discretization of motion equation

Eq. (6) shows that differential equation of structure oscillation is coupled to nonlinear van der Pol wake oscillator. Therefore the Galerkin method is used to discretize the equation of motion. Firstly, the exact mode shape of free vibration of system, i.e., the mode shape considering the non-uniformity of the cross section, is extracted to be used as comparison function. Therefore, the free vibration response of system is assumed as

$$\begin{aligned}&w(x,t)=\varphi_{i,1}(x)e^{i\omega_i t},\quad x\le\frac{l_1}{l},\\&w(x,t)=\varphi_{i,2}(x)e^{i\omega_i t},\quad x\ge\frac{l_1}{l}\end{aligned} \tag{8}$$

Where $\varphi_{i,1}(x)$ and $\varphi_{i,2}(x)$ are the functions of *i*-th mode shape along the rod and cylinder length. Substituting Eq. (8) into Eq. (1) without considering the damping and wake oscillator term results in

$$\begin{aligned}&-\omega_i^2\varphi_{i,1}(x)+\frac{d^4\varphi_{i,1}(x)}{dx^4}=0, && x\le\frac{l_1}{l},\\&-\left(\frac{\rho_2 A_2}{\rho_1 A_1}\right)\omega_i^2\varphi_{i,2}(x)+\left(\frac{E_2 I_2}{E_1 I_1}\right)\frac{d^4\varphi_{i,2}(x)}{dx^4}=0 && \frac{l_1}{l}<x<1\end{aligned} \tag{9}$$

By solving the above equations, $\varphi_{i,1}$ and $\varphi_{i,2}$ will be as follows

$$\begin{aligned}&\varphi_{i,1}(x)=C_1\cosh(\beta_{1,i}x)+C_2\sinh(\beta_{1,i}x)+C_3\cos(\beta_{1,i}x)+C_4\sin(\beta_{1,i}x),\quad x\le\frac{l_1}{l},\\&\varphi_{i,2}(x)=C_5\cosh(\beta_{2,i}x)+C_6\sinh(\beta_{2,i}x)+C_7\cos(\beta_{2,i}x)+C_8\sin(\beta_{2,i}x),\quad x\ge\frac{l_1}{l},\\&\beta_{1,i}=\sqrt{\omega_i},\qquad \beta_{2,i}=\left(\frac{\rho_2 A_2 E_1 I_1}{\rho_1 A_1 E_2 I_2}\omega_i^2\right)^{\frac{1}{4}}\end{aligned} \tag{10}$$

where C_i are constant coefficients, calculated from boundary and continuity conditions due to equality of shear and moment at the stepped cross section as

$$\begin{aligned}&\varphi_{i,1}\big|_{x=0}=0,\quad \frac{d\varphi_{i,1}}{dx}\bigg|_{x=0}=0,\quad \frac{d^2\varphi_{i,2}}{dx^2}\bigg|_{x=1}=0,\quad \frac{d^3\varphi_{i,2}}{dx^3}\bigg|_{x=1}=0\\&\varphi_{i,1}\big|_{x=l_1/l}=\varphi_{i,2}\big|_{x=l_1/l},\quad \frac{d\varphi_{i,1}}{dx}\bigg|_{x=l_1/l}=\frac{d\varphi_{i,2}}{dx}\bigg|_{x=l_1/l},\\&\frac{d^2\varphi_{i,1}}{dx^2}\bigg|_{x=l_1/l}=\left(\frac{E_2 I_2}{E_1 I_1}\right)\frac{d^2\varphi_{i,2}}{dx^2}\bigg|_{x=l_1/l},\quad \frac{d^3\varphi_{i,1}}{dx^3}\bigg|_{x=l_1/l}=\left(\frac{E_2 I_2}{E_1 I_1}\right)\frac{d^3\varphi_{i,2}}{dx^3}\bigg|_{x=l_1/l}\end{aligned} \tag{11}$$

Therefore, system normalized mode shape will be

$$\Phi_i(x)=\frac{\left(1-\mathrm{H}(x-\frac{l_1}{l})\right)\varphi_{i,1}(x)+\mathrm{H}(x-\frac{l_1}{l})\varphi_{i,2}(x)}{\sqrt{\int_0^1 m(x)((1-\mathrm{H}(x-\frac{l_1}{l}))\varphi_{i,1}(x)+\mathrm{H}(x-\frac{l_1}{l})\varphi_{i,2}(x))^2 dx}} \tag{12}$$

The main part of the structure oscillation belongs to the first mode shape; therefore it may be assumed that $w(x,t)=\Phi_1(x)p(t)$ and $Q(x,t)=\Phi_1(x)q(t)$ where $\Phi_1(x)$ is the first normalized mode shape. In addition $p(t)$ and $q(t)$ are time coordinate functions correspond to structure and wake oscillations, respectively. By substituting these assumptions into Eq. (6), multiplying the outcome by $\Phi_1(x)$ and integrating on the whole length of the structure, the differential equation governing the system oscillations will be as

$$\begin{aligned}&\frac{d^2 p(\tau)}{d\tau^2}+c_{eq}\Omega_f\frac{dp(\tau)}{d\tau}+\omega_s^2 p(\tau)=f_{eq}\Omega_f^2 q(\tau),\\&\frac{d^2 q(\tau)}{d\tau^2}+\eta\Omega_f(S\,q^2(\tau)-1)\frac{dq(\tau)}{d\tau}+\Omega_f^2 q(\tau)=G\frac{d^2 p(\tau)}{d\tau^2}\\&\omega_s=(\int_0^1\Phi_1(x)\bar{E}(x)\bar{I}(x)\frac{\partial^4\Phi_1(x)}{\partial x^4}dx)^{0.5},\qquad c_{eq}=\int_0^1\bar{c}(x)\Phi_1^2(x),\\&f_{eq}=\int_0^1\bar{f}(x)\Phi_1^2(x)(Heaviside(x-\frac{l_1}{l}))dx,\qquad S=\frac{\int_{\frac{l_1}{l}}^1\Phi_1^3(x)dx}{\int_{\frac{l_1}{l}}^1\Phi_1(x)dx}\end{aligned} \tag{13}$$

where $\omega_s=\omega_1$ is the first natural frequency of vibration of the structure.

4. Frequancy and modal analysis

Neglecting the nonlinear and damping terms, the motion equations governing the oscillations will be as

$$\begin{aligned}&\frac{d^2 p(\tau)}{d\tau^2}+\omega_s^2 p(\tau)=f_{eq}\Omega_f^2 q(\tau),\\&\frac{d^2 q(\tau)}{d\tau^2}+\Omega_f^2 q(\tau)=G\frac{d^2 p(\tau)}{d\tau^2}\end{aligned} \tag{14}$$

Now, considering the response of Eq. (14) as $(p(\tau),q(\tau))=(\bar{p},\bar{q})e^{i\nu\tau}$ and substituting it into Eq. (14)

$$(-\nu^2+\omega_s^2)\bar{p}-f_{eq}\Omega_f^2\bar{q}=0,\quad G\nu^2\bar{p}+(-\nu^2+\Omega_f^2)\bar{q}=0 \tag{15}$$

For nonzero solution the determinant of coefficients must be equal to zero, so

$$\nu^4-(\omega_s^2+\Omega_f^2-f_{eq}G\Omega_f^2)\nu^2+\omega_s^2\Omega_f^2=0 \tag{16}$$

By solving the algebraic Eq. (16), it results to the following frequencies and modal shapes

$$2(\nu_\pm)^2=(\omega_s^2+\Omega_f^2-f_{eq}G\,\Omega_f^2)\pm\sqrt{(\omega_s^2+\Omega_f^2-f_{eq}G\,\Omega_f^2)^2-4\omega_s^2\Omega_f^2},\quad \frac{\bar{p}}{\bar{q}}=\frac{f_{eq}\Omega_f^2}{(-\nu^2+\omega_s^2)}=\frac{(-\nu^2+\Omega_f^2)}{G\nu^2} \tag{17}$$

When the value of expression inside the radical is positive, then both values for ν will be real, and therefore both solution modes, i.e., $e^{i\nu_1\tau}, e^{i\nu_2\tau}$, will be periodic. When the value of expression inside the radical is negative, then the mode with negative imaginary part of ν will be unstable. So the boundary values of Ω_f for staying in unstable domain may be obtained by letting the expression inside the radical equal to zero as follows

$$(\omega_s^2+(1-f_{eq}G)\Omega_f^2)^2-4\omega_s^2\Omega_f^2=0,\quad \Omega_{f\pm}=\frac{\omega_s}{1\pm\sqrt{f_{eq}G}} \tag{18}$$

In the range of $\Omega_{f+}<\Omega_f<\Omega_{f-}$, the linear system is unstable. Noting Eq. (7) which demonstrates that $\Omega_f=2\pi S_T UT/D$, the boundary values for unstable solution based on the wind speed will be as

$$U=\frac{D}{2\pi TS_T}\frac{\omega_S}{1\pm\sqrt{f_{eq}G}}=\frac{D}{2\pi S_T}\frac{\Omega_S}{1\pm\sqrt{f_{eq}G}},\quad \Omega_S=\frac{\omega_S}{T} \tag{19}$$

Where Ω_S is the first dimensional natural frequency of system and, as mentioned before, ω_S is the first non-dimensional natural frequency. It has been shown by de Langre (2006) that, for a rigid cylinder mounted on the spring, the unstable domain of linear system corresponds to lock-in domain.

5. Solving the equation using multiple scales method

It has been shown in previous section that, if the one neglects the effect of linear damping and also nonlinear van der Pol damping coupling terms of Eq. (13), then system will be unstable for a range of wind speed. It means that the amplitude of structure oscillations tends to infinity in that range, which is not physically acceptable. Therefore, to get a true solution, the coupled linear terms must be balanced with nonlinear and damping terms. So that, to strike a balance between the terms of Eq. (13), the bookkeeping parameter $\varepsilon=1$, which represents the order of terms, is used as below

$$\frac{d^2p(\tau)}{d\tau^2}+\varepsilon c_{eq}\Omega_f\frac{dp(\tau)}{d\tau}+\omega_s^2p(\tau)=\varepsilon f_{eq}\Omega_f^2q(\tau),\quad \frac{d^2q(\tau)}{d\tau^2}+\varepsilon\eta\Omega_f(Sq^2(\tau)-1)\frac{dq(\tau)}{d\tau}+\Omega_f^2q(\tau)=\varepsilon G\frac{d^2p(\tau)}{d\tau^2} \tag{20}$$

Now the response of Eq. (20) is assumed as follows using multiple scales method of perturbation theory

$$P(\tau)=p_0(T_0,T_1)+\varepsilon p_1(T_0,T_1),\quad q(\tau)=q_0(T_0,T_1)+\varepsilon q_1(T_0,T_1) \tag{21}$$

Where $T_0=\tau$ and $T_1=\varepsilon\tau$ are time scales. By substituting Eq. (21) into Eq. (20) and separating terms with equal order of ε, the following relations are obtained:

Order (1)

$$\frac{d^2}{dT_0^2}p_0(T_0,T_1)+\omega_s^2p_0(T_0,T_1)=0,\quad \frac{d^2}{dT_0^2}q_0(T_0,T_1)+\Omega_f^2q_0(T_0,T_1)=0 \tag{22}$$

Order (ε)

$$\frac{\partial^2}{\partial T_0^2}p_1(T_0,T_1)+\omega_s^2p_1(T_0,T_1)=-2\frac{\partial^2p_0(T_0,T_1)}{\partial T_0\partial T_1}-c_{eq}\Omega_f\frac{\partial p_0(T_0,T_1)}{\partial T_0}+f_{eq}\Omega_f^2q_0(T_0,T_1),$$
$$\frac{\partial^2}{\partial T_0^2}q_0(T_0,T_1)+\Omega_f^2q_0(T_0,T_1)=-2\frac{\partial^2q_0}{\partial T_0\partial T_1}-\eta\Omega_f(\mathrm{S}q_0^2(T_0,T_1)-1)\times\frac{\partial q_0(T_0,T_1)}{\partial T_0}+G\frac{\partial^2p_0(T_0,T_1)}{\partial T_0^2} \tag{23}$$

The solution of Eq. (23) will be as follows

$$p_0(T_0,T_1)=A(T_1)e^{i\omega_sT_0}+\bar{A}(T_1)e^{-i\omega_sT_0},\quad q_0(T_0,T_1)=B(T_1)e^{i\Omega_fT_0}+\bar{B}(T_1)e^{-i\Omega_fT_0} \tag{24}$$

Whereas $A(T_1)$ and $B(T_1)$ are the complex coefficients and $\bar{A}(T_1)$ and $\bar{B}(T_1)$ are their complex conjugates. These coefficients are obtained by solvability conditions applied in the following process. By substituting Eq. (24) into Eq. (23)

$$\frac{\partial^2}{\partial T_0^2}p_1(T_0,T_1)+\omega_s^2p_1(T_0,T_1)=-2\omega_s\,\mathrm{i}(\frac{\partial A(T_1)}{\partial T_1}e^{i\omega_sT_0}-\frac{\partial\bar{A}(T_1)}{\partial T_1}e^{-i\omega_sT_0})-c_{eq}\Omega_f(A(T_1)i\omega_se^{i\omega_sT_0}-\bar{A}(T_1)i\omega_se^{-i\omega_sT_0})+f_{eq}\Omega_f^2(B(T_1)e^{i\Omega_fT_0}+\bar{B}(T_1)e^{-i\Omega_fT_0}),$$
$$\frac{\partial^2}{\partial T_0^2}q_1(T_0,T_1)+\Omega_f^2q_1(T_0,T_1)=-2\Omega_f\,\mathrm{i}(\frac{\partial B(T_1)}{\partial T_1}e^{i\Omega_fT_0}-\frac{\partial\bar{B}(T_1)}{\partial T_1})e^{-i\Omega_fT_0}-\eta\Omega_f(S(B(T_1)e^{i\Omega_fT_0}+\bar{B}(T_1)e^{-i\Omega_fT_0})^2-1)(i\Omega_fB(T_1)e^{i\Omega_fT_0}-i\Omega_f\bar{B}(T_1)e^{-i\Omega_fT_0})+G(-A(T_1)\omega_s^2e^{i\omega_sT_0}-\bar{A}(T_1)\omega_s^2e^{-i\omega_sT_0}) \tag{25}$$

By assuming $\Omega_f=\omega_s+\varepsilon\sigma$, whereis the detuning σ parameter, and by rearranging the outcome

$$\frac{\partial^2}{\partial T_0^2}p_1(T_0,T_1)+\omega_s^2p_1(T_0,T_1)=(-2\omega_s\frac{\partial A(T_1)}{\partial T_1}i-c_{eq}\Omega_fA(T_1)i\omega_s+f_{eq}\Omega_f^2B(T_1)e^{i\sigma\varepsilon T_0})e^{i\omega_sT_0}+NST+cc,$$
$$\frac{\partial^2}{\partial T_0^2}q_1(T_0,T_1)+\Omega_f^2q_1(T_0,T_1)=(-2i\Omega_f\frac{\partial B(T_1)}{\partial T_1}-\eta S\Omega_f^2B^2(T_1)\bar{B}(T_1)i+\eta\Omega_f^2B(T_1)\mathrm{i}-G\omega_s^2A(T_1)e^{-\varepsilon\sigma T_0i})e^{i\Omega_fT_0}+NST+cc \tag{26}$$

CC indicates conjugate of complex term, and *NST* represents all terms which are not secular. For solvability condition the coefficient of secular term in Eq. (26), i.e., the coefficients of $e^{i\omega_s T_0}$ and $e^{i\Omega_f T_0}$ must become equal to zero. By equating it to zero and substituting $A(T_2)$ as polar, $A(T_1)=\frac{1}{2}a(T_1)e^{i\alpha(T_1)}$, and $B(T_1)=\frac{1}{2}b(T_1)e^{i\beta(T_1)}$, and noting that $\varepsilon T_0 = T_1$, one obtains

$$\begin{aligned}
&-\dot{a}\omega_s e^{i\alpha} i + a\dot{\alpha}\omega_s e^{i\alpha} - \frac{c_{eq}\Omega_f}{2} i a\omega_s e^{i\alpha} + \frac{f_{eq}\Omega_f^2}{2} b e^{i\beta} e^{i\sigma T_1} = 0,\\
&-\Omega_f \dot{b} e^{i\beta} i + \Omega_f \dot{\beta} b e^{i\beta} - \frac{\eta S\Omega_f^2}{8} b^3 i e^{i\beta} + \frac{\eta\Omega_f^2}{2} b i e^{i\beta} - \frac{G\omega_s^2 a}{2} e^{i\alpha} e^{-i\sigma T_1} = 0
\end{aligned} \tag{27}$$

By multiplying $e^{-i\alpha}$ at the first equation and multiplying $e^{-i\beta}$ at the second equation

$$\begin{aligned}
&-\dot{a}\omega_s i + a\dot{\alpha}\omega_s - \frac{c_{eq}\Omega_f}{2} i a\omega_s + \frac{f_{eq}\Omega_f^2}{2} b e^{i(\beta-\alpha+\sigma T_1)} = 0,\\
&-\Omega_f \dot{b} i + \Omega_f \dot{\beta} b - \frac{\eta S\Omega_f^2}{8} b^3 i + \frac{\eta\Omega_f^2}{2} b i - \frac{G\omega_s^2 a}{2} e^{i(\alpha-\beta-\sigma T_1)} = 0
\end{aligned} \tag{28}$$

By separating the real part and imaginary part of Eq. (28) and equating the outcome equal to zero

$$\begin{aligned}
\dot{\alpha} &= \frac{-f_{eq}\Omega_f^2}{2a\omega_s} b\cos(\beta-\alpha+\sigma T_1),\\
\dot{a} &= -\frac{c_{eq}\Omega_f}{2} a + \frac{f_{eq}\Omega_f^2}{2\omega_s} b\sin(\beta-\alpha+\sigma T_1),\\
\dot{\beta} &= \frac{G\omega_s^2 a}{2\Omega_f b}\cos(\alpha-\beta-\sigma T_1)\\
\dot{b} &= -\frac{\eta\Omega_f b}{8}(S b^2-4) - \frac{G\omega_s^2 a}{2\Omega_f}\sin(\alpha-\beta-\sigma T_1)
\end{aligned} \tag{29}$$

Now by assuming $\psi = \beta-\alpha+\sigma T_1$

$$\begin{aligned}
\dot{\psi} &= \left(\frac{G\omega_s^2 a}{2\Omega b} + \frac{f_{eq}\Omega_f^2 b}{2a\omega_s}\right)\cos(\psi) + \sigma\\
\dot{a} &= -\frac{c_{eq}\Omega_f}{2} a + \frac{f_{eq}\Omega_f^2}{2\omega_s} b\sin(\psi),\\
\dot{b} &= -\frac{\eta\Omega_f b}{8}(S b^2-4) + \frac{G\omega_s^2 a}{2\Omega_f}\sin(\psi)
\end{aligned} \tag{30}$$

By putting derivative of a, b and ψ equal to zero in Eq. (30), the equation governing equilibrium solution amplitude will be obtained. If one substitutes $A(T_1)$ and $B(T_1)$ into Eq. (24)

$$\begin{aligned}
p_0(T_0,T_1) &= \frac{1}{2}a(T_1)e^{i\alpha(T_1)}e^{i\omega_s T_0} + \frac{1}{2}a(T_1)e^{-i\alpha(T_1)}e^{-i\omega_s T_0}\\
q_0(T_0,T_1) &= \frac{1}{2}b(T_1)e^{i\beta(T_1)}e^{i\Omega_f T_0} + \frac{1}{2}b(T_1)e^{-i\beta(T_1)}e^{-i\Omega_f T_0}
\end{aligned} \tag{31}$$

The above equation demonstrates that when the effect of damping is considered, then the frequency presented in wake and structure oscillation are as $\dot{\alpha}+\omega_s$ and $\dot{\beta}+\Omega_f$, respectively.

6. Numerical solution

The equations of motion (20) are solved using R*unge–Kutta–Fehlberg* numerical method, which is called RKF45. Variations of steady state amplitudes of the structure and wake oscillations with respect to the variations of wind speed are extracted for two loops of wind speed. During the first loop, the value of Ω_f, which is closely related to the wind speed, is considered much less than the natural frequency of linear system. Then, solving the equations of motion and by obtaining time history of solution, the amplitude of the steady state is recorded. By slightly increasing the value of Ω_f i.e., by slowly increasing the wind speed, the previous step is repeated. The steady-state amplitude of the previous step is considered as the initial conditions of displacement for the next step, whilst the initial condition of the velocity is settled to zero. This loop is followed until Ω_f largely overpass the system natural frequency. Once terminated this loop, the same operations is repeated for the second loop by slowly decreasing the value of Ω_f. The backward loop is followed until Ω_f reaches the same value of Ω_f at the beginning of forward loop. The importance of sweeping the frequency during the forward loop and the backward loop is due to the fact that a system under vortex induced vibration has a hysteresis behavior. It causes, in fact, the sudden oscillation amplitude at a frequency which is different during forward and backward loop.

7. Results and discussion

In this part, the effects of system parameters change are studied in terms of structure oscillation amplitude and wake oscillation amplitude. The system parameters are considered as in Table 1, except for those values which are written on the caption (or legend) of each figure. Also it must be noted that when the fluid is water then $C_M = 1$ (Facchinetti *et al.* 2004b), and when the fluid is air the amount of added mass may be negligible due to low value of air mass density, even if one assumes $C_M = 1$. For stationary cylinder in the sub-critical range $300 < \mathrm{Re} < 1.5\times10^5$ the amount of C_D can be assumed 1.2 (Facchinetti *et al.* 2004a). It should be also remarked that the drag coefficient becomes nonlinear when it is referred to oscillations in transverse direction. However, for the sake of simplicity, C_D was assumed equal to 2 by de Langre (2006); so far, noting that the Strouhal number (S_T) is equal to 0.2 in $300 < \mathrm{Re} < 1.5\times10^5$ (Blevins 1990), the value of γ will be equal to 0.8.

Table 1 Parameters of system

$l(m)$	$l_1(m)$	$\rho_1(kg/m^3)$	$\rho_2(kg/m^3)$	$\rho_f(kg/m^3)$
1	0.3	2700	2700	1.2
$E_1(N/m^2)$	$E_2(N/m^2)$	$d(m)$	$D(m)$	$h(m)$
70×10^9	70×10^9	0.005	0.1	5×10^{-4}

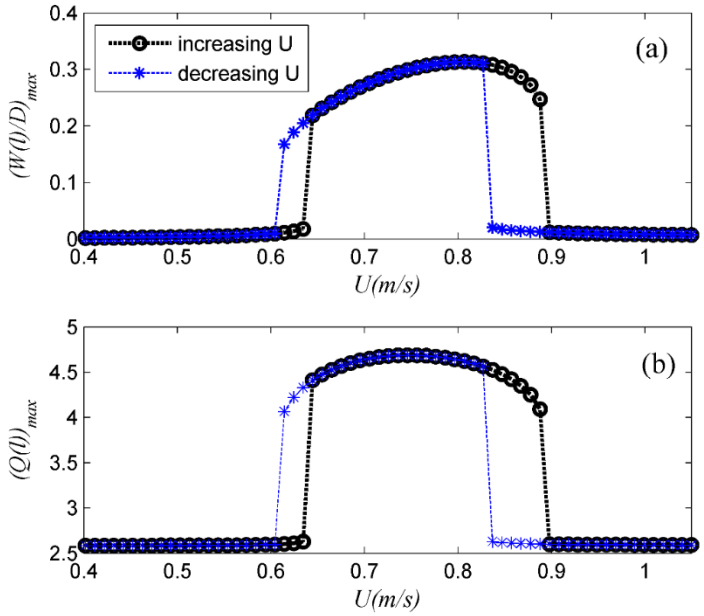

Fig. 2 (a) is the variation of the steady state amplitude of the structure oscillation, and (b) is the variation of wake oscillation amplitude with respect to the variation of wind speed at the free end of the structure

Fig. 2 shows the steady state amplitude of the structure oscillations and wake oscillations with respect to the variation of wind speed using numerical method. It shows that, for low values of wind speed, the structure oscillation amplitude remains very small whilst, by slowly increasing the wind speed, a "special" value is reached when the amplitude suddenly increases to a large value.

Graphs also show that further increasing the wind speed value the amplitude remains large until a second "special" value is reached, when the amplitude suddenly decreases to a very small value; this interval is called lock-in domain. It is shown in Fig. 2 that a similar behavior takes place by decreasing the wind speed. It also indicates that, along the decreasing wind speed phase, the wind speed corresponding to sudden variation of the amplitude are different. In other worlds, a hysteresis phenomenon between the forward and backward loops evidently appears.

It is shown in Fig. 3 that there is a reasonable agreement between the results obtained by the numerical and the perturbation method. The comparison of Figs. 2(a) and 2(b) shows that the trend of the variation of the structure oscillations amplitude and the trend of the variation of the wake oscillations amplitude are similar. However, in contrast with structure oscillation, whose amplitude outside the lock-in domain is very small, the amplitude of the wake oscillation remains considerably high even outside the cited domain. This is shown in Fig. 4, where the time history of structure and wake oscillation are depicted in dimensionless time domain. Fig. 4(b) shows that, although the amplitude of the wake oscillator is considerable for $U = 0.6m/s$, the structure oscillation is very small. By increasing the wind speed to $0.75m/s$, the amplitude of the wake oscillation, and specially the amplitude of the structure oscillation, increases significantly.

The main reason of increasing structure oscillations may be found in the variations of frequency of the wake oscillations due to interaction between wind and structure shown in Fig. 5. It indicates that if the flexibility of the structure is neglected i.e., it is assumed as a constrained rigid cylinder without oscillation, then according to Strouhal number, the vortex shedding frequency increases by increasing the wind speed. It must be mentioned that when the fluid passes over a constrained rigid cylinder, the frequency of vortex shedding may be evaluated using Strouhal number as $U.S_T/D$ in Hz (Facchinetti *et al.* 2004a), and in dimensionless form as $2\pi.T.U.S_T/D$. If the flexibility of the structure be considered then, according to

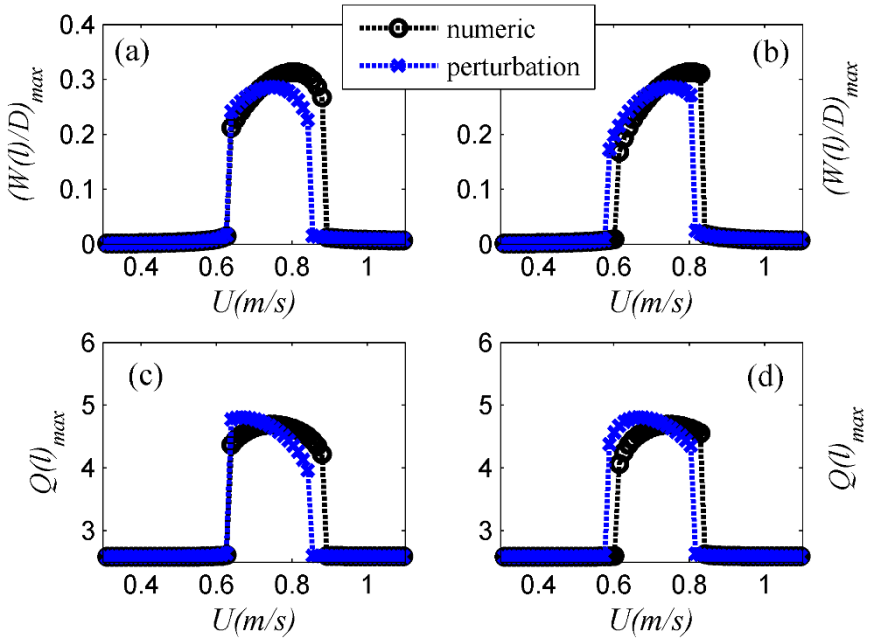

Fig. 3 Comparison between numerical method and multiple scale perturbation method at the free end of the system, (a) and (b) belong to structure oscillation by increasing and decreasing wind speed, respectively and (c) and (d) belong to the wake oscillation

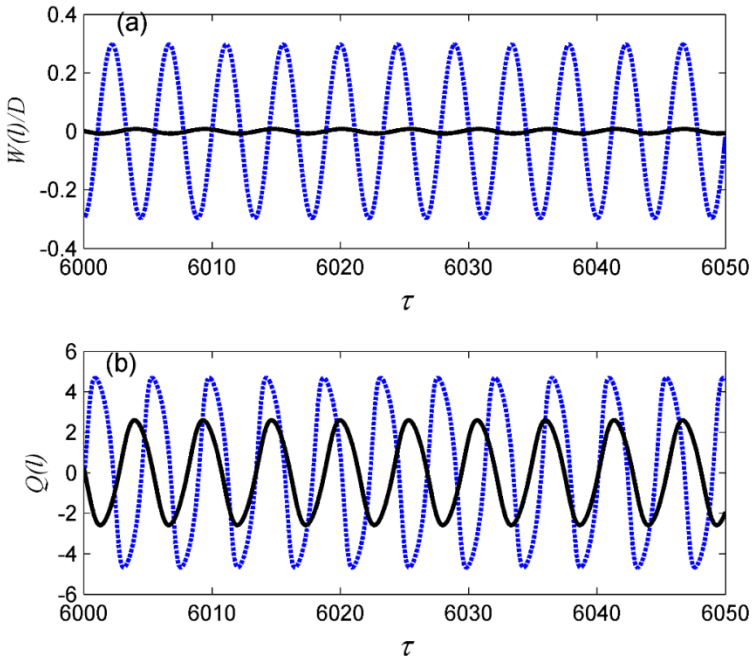

Fig. 4 (a) is time history of the structure oscillation of the free end of the system, and (b) is time history of the wake oscillation, solid line is for $U = 0.6m/s$, and dashed line is for $U = 0.75m/s$ resulted from numeric solution

Eq. (24), the frequency of vortex shedding will be as $\Omega_f + \dot{\beta}$. Fig. 5 shows that the vortex shedding frequency is locked on the natural frequency of the structure for a special domain of the wind speed. It demonstrates that outside of this domain the frequency of vortex shedding follows the predicted value by Strouhal number. The domain where vortex synchronizes itself to the natural frequency of the structure is called lock-in domain (Facchinetti *et al*. 2004a). It causes the structure oscillating with a large amplitude.

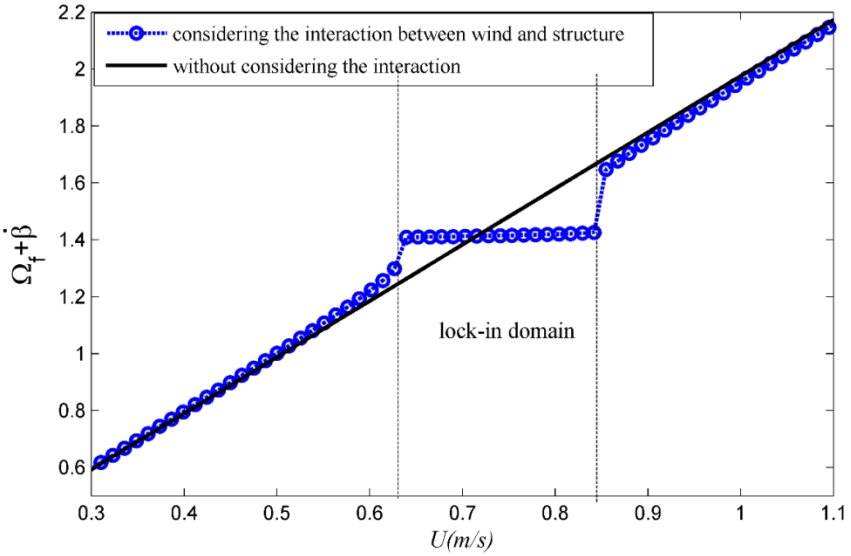

Fig. 5 Variations of the frequency of the wake oscillator with respect to the variations of wind speed with considering damping and nonlinear terms according to the perturbation solution

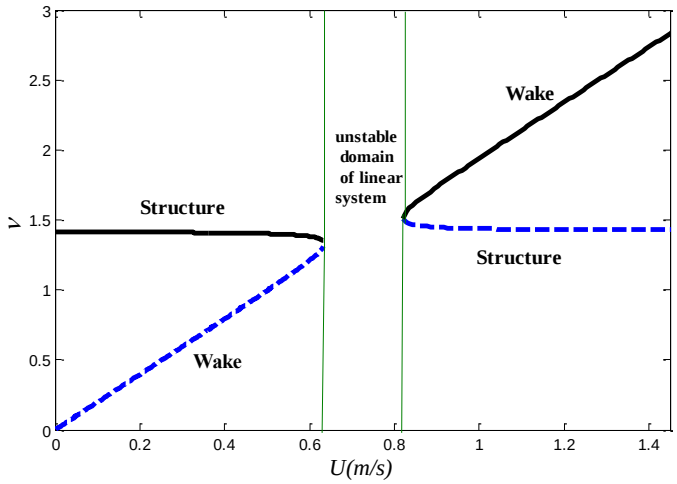

Fig. 6 Eigenvalue variations of linear system with respect to the variations of wind speed

Concisely, the comparison between vortex shedding frequency for rigid cylinder and for the flexible structure here considered shows that outside the lock-in range the predicted values are approximately identical, since no interaction subsists between wind and structure oscillation. It also demonstrates that along the lock-in range their values are different, due to the interaction between wind and flexible structure.

Now the relation between lock-in domain and instability domain of undamped linear system is considered. The variations of the eigenvalue of the undamped linear system with respect to the wind speed are shown in Fig. 6 using Eq. (17). It is clear that system has two different eigenvalues for low values of wind speed. By increasing the wind speed value the eigenvalue related to the wake oscillator increases up to approximately equalize the natural frequency. After this value, the linear system becomes unstable until two real eigenvalues appear again. A comparison between Figs. 6 and 5 shows that the lock-in domain of Fig. 5 corresponds to the unstable domain of Fig. 6. It shows that although a good prediction of lock-in domain may be extracted by linear system, it is not possible to predict the amplitude of structure and wake oscillation. The results demonstrate that both lock-in domain and amplitude can be predicted using analytical multiple scale perturbation method. It has been shown in the last paragraph of previous section that when the damping effect is considered then the frequency of structure and wake oscillation are $\dot{\alpha}+\omega_s$ and $\dot{\beta}+\Omega_f$, respectively. Noting Eq. (30) when the response of system reaches the steady state condition, then $\dot{\psi}=\dot{\beta}-\dot{\alpha}+\sigma=0$. In applying perturbation method it was assumed that

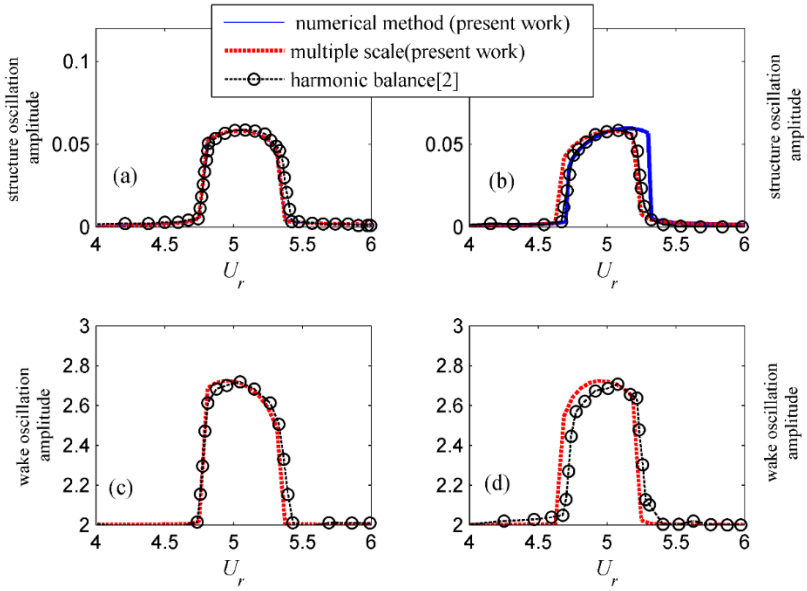

Fig. 7 Amplitude of the structure oscillations and wake oscillation for a rigid cylinder mounted on the spring (a) and (c) belong to wind speed increasing and (c) and (d) belong to wind speed decreasing

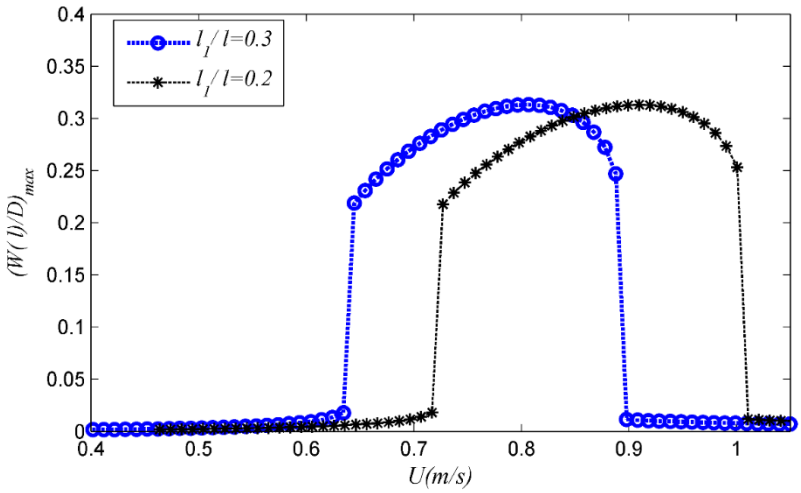

Fig. 8 Variations of steady state amplitude of the structure oscillations at its free end with respect to the variations of wind speed for different values of the first cylinder length

$\Omega_f = \omega_s + \sigma$. By combining these assumptions, it is evidenced that the frequency appearing in wake and structure oscillation are identical. It means that the variations of dominant frequency of structure oscillation follow the curve shown by circle points in Fig. 5. The comparison between Figs. 5 and 6 demonstrates that one of the mode predicted by linear modal analysis is damped when the effect of damping factor is taken into account. As shown in Fig. 5, it means that outside the lock-in domain the dominant frequency belongs to the wake and inside the lock-in domain it belongs to the structure.

For special coefficients of $F_{eq} = 0.0002, \eta = 0.3, \mathrm{S} = 1$ and $G = 12$ of Eq. (13), and replacing c_{eq} by $2\zeta + \gamma / \mu$, and $\Omega_f = S_T U_r$ where $\zeta = 0.0031, \gamma = 0.8$ and $\mu = 250$ the equation of motion corresponds to the dimensionless motion equation of the rigid cylinder mounted on the flexible spring, and studied by de Langre (2006) and (Facchinetti *et al.* (2004a). They solved the equations of motion using harmonic balance, i.e., considering only the main harmonic contribution. Fig. 7 shows a comparison of the present work to the results presented by Facchinetti *et al.* (2004a) demonstrating a good agreement between the results.

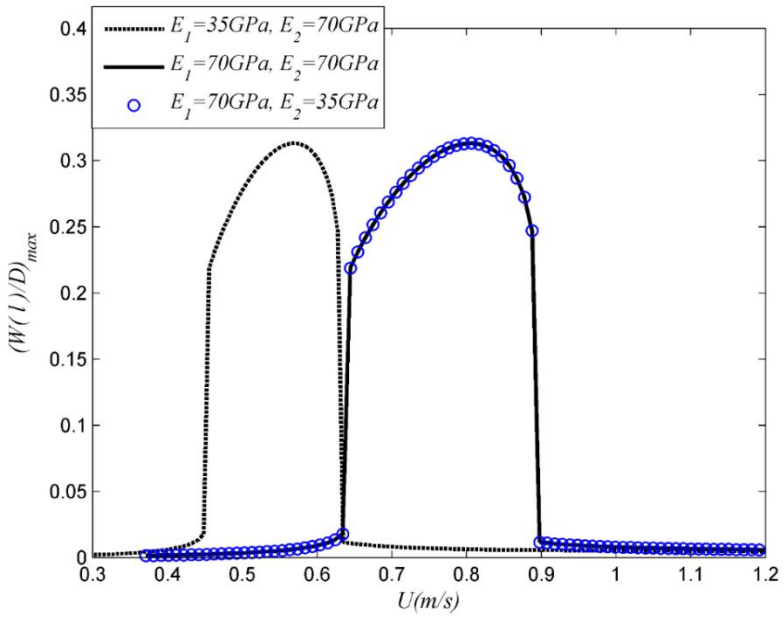

Fig. 9 Variations of steady state amplitude of the structure oscillations at its free end with respect to the variations of wind speed for different values of elasticity modulus

Fig. 8 shows the effect of increasing the length of the rod, l_1, on the steady state amplitude of the structure oscillations. It indicates that by increasing the value of l_1, i.e. reducing its stiffness, the lock-in starts sooner and the span of lock-in domain decreases. This is simply due to the fact that according to Eq. (13) by increasing of the value of l_1, the stiffness reduces and hence the value of natural frequency Ω_s decreases too. Considering Eq. (18) the upper and lower range of the lock-in domain decrease by lowering the value of the natural frequency.

Fig. 9 shows that the variations of lock-in domain and steady state amplitude of the structure oscillation are not considerable when the mounted cylinder elasticity modulus changes. The reason is that the main contribution of structure oscillations belongs to its first mode shape. As shown in Fig. 10, the structure curvature along the mounted cylinder length related to its first mode is negligible. It is mainly due to the large value of the second area moment of the cylinder, i.e., it means that cylinder is approximately animated by a rigid motion. Therefore, an increase of the modulus of the cylinder does not have visible effect on the oscillation of the structure. Fig. 9, on the contrary, indicates that the change of the based rod elasticity modulus has a relevant effect on the values of lock-in domain. As expected, it shows that increasing the value of based rod elasticity modulus the lock-in domain begins at higher wind speed. Moreover, even the range of lock-in phenomenon increases; the amplitude does not shows a considerable change. It is due to the fact that the curvature of the structure at the part near to the clamped boundary is considerable and so a change of its elasticity modulus causes the change of structure oscillation.

Fig. 11 indicates that by increasing the diameter of the cylinder, the lock-in range starts at larger wing speed. Moreover, it shows that the span of the lock- in domain increases. It has been mentioned that the frequency of vortex shedding outside the lock-in domain can be evaluated using Strouhal number as $U.ST/D$ in Hz. When the predicted value by Strouhal number approaches the natural frequency of the structure, vortex shedding frequency deviates from Strouhal relation and becomes locked on the natural frequency (Facchinetti *et al.* 2004a). According to equation $U.ST/D$ that predicts the vortex shedding frequency outside of lock-in domain, it clearly appears that by increasing the cylinder diameter the vortex frequency decreases. Therefore, if the diameter of the cylinder increases, a larger value of wind speed is required to get the vortex shedding frequency equal to the natural frequency and, consequently, the lock-in phenomenon to take place. The effect of the change of the value of fluid mass density on the structure oscillation amplitude is shown in Fig. 12. It shows that, in contrast to previous figures, the lock-in domain enlarges on both sides. In other words, the lock-in domain ~~will~~ becomes wider by increasing fluid density. This result is in agreement with the previous works outcomes for rigid mass cylinder mounted on a flexible spring (Facchinetti *et al.* 2004a). It has been also shown in that work that, by decreasing the ratio of $m_s/\rho_f D^2$ (where m_s is the mass of structure), the range of lock-in becomes wider. It is hence clear that a lowering of the ρ_f value leads to the opposite effect.

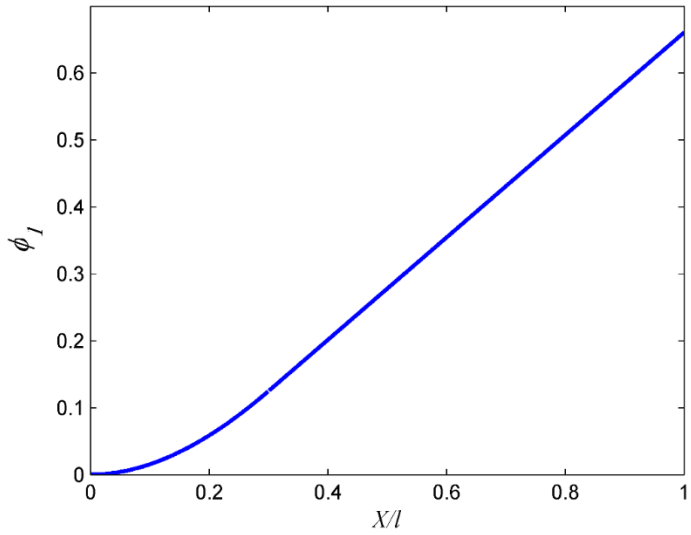

Fig. 10 The first natural mode shape of system

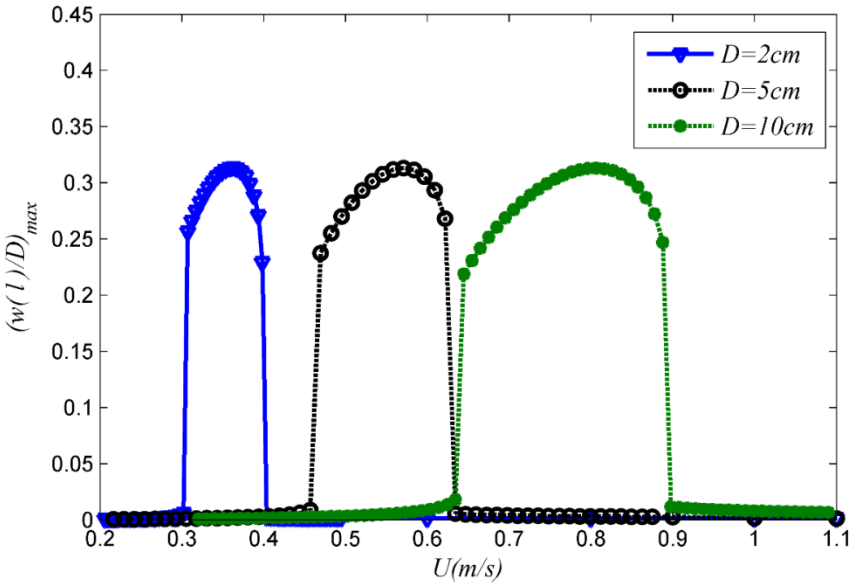

Fig. 11 Variations of the steady state amplitude of the structure oscillations at its free end with respect to the variations of wind speed for different values of mounted cylinder diameter

The drag coefficient and Strouhal number are dimensionless number and do not depend on the fluid; so that here, similarly to previous work (de Langre 2006), it was assumed that $\gamma = 0.8$. However, since the value of drag coefficient may be changed when it is referred to oscillations in transverse direction (Facchinetti *et al.* 2004a), the effect of variations of γ is presented in Fig. 13. It shows that by increasing γ, the steady state amplitude of the structure oscillations increases, and the lock-in domain becomes wider. It demonstrates that the effect of γ on the structure oscillation is considerable. It means that an error in evaluating γ may results in a considerable computational error. Therefore, by considering the effect of this parameter over the considered application, a key element of bladeless wind turbine adoption, future works should be focused on this subject. It becomes even more relevant, when we consider that most of previous semi-empirical models have been developed based on experimental information of water and not air.

8. Conclusions

The lock-in phenomenon and the non-linear response of a flexible cylinder mounted on a flexible rod has been modelled

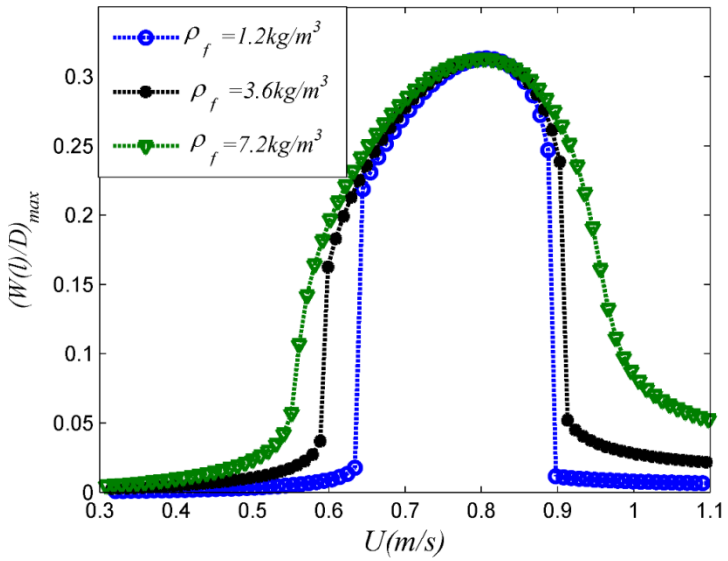

Fig. 12 Variations of steady state amplitude of the structure oscillations at its free end with respect to the variations of wind speed for different values of mass fluid density

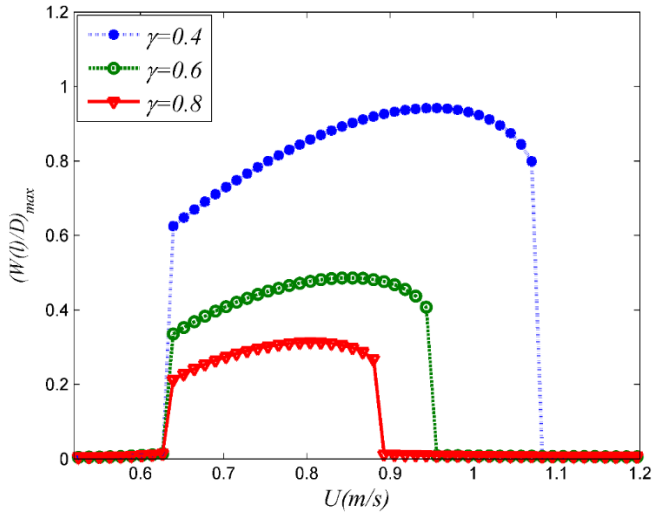

Fig. 13 Variations of steady state amplitude of the structure oscillations at its free end with respect to the variations of wind speed for different values of stall parameter γ

based on wake model proposed by Facchinetti *et al.* (2004a). The equations of motion have been discretized by Galerkin method using exact mode shape of system as comparison function, and then solved using both the RKF45 numerical method and the analytical perturbation method. The results demonstrate a good agreement between the multiple scale and numerical method results. An analytical expression that predicts the lock-in phenomenon range of wind speed is derived.

The results also show that the linear system is unstable in the wind speed span which corresponds to the lock-in domain of the non-linear system. It has been shown that the starting and stopping points of the lock-in domain are different when the wind speed is increasing or it is decreasing. It has been shown that, by lowering the natural frequency of system (for instance by decreasing the elasticity modulus of the foundation rod or by increasing its length or even by increasing the mass of the cylinder) the lock-in domain starts sooner, and its span decreases. It has also been shown that, by decreasing the diameter of the mounted cylinder the lock-in domain starts sooner. Moreover, the span domain and the amplitude of the structure oscillations decreases. The results also indicate

that by increasing the fluid density the lock-in domain starts sooner and stops later.

For some special parameters, the equation of motion of this paper corresponds to the motion equation of the rigid cylinder mounted on the flexible spring and studied by Facchinetti *et al.* (2004a). Results are in good agreement with those published on previous works and obtained by a harmonic balance approach.

References

Abdelkefi, A., Yan, Z. and Hajj, M.R. (2013), "Modeling and nonlinear analysis of piezoelectric energy harvesting from transverse galloping", *Smart Mater Struct.*, **22**(1), 025016.

Abdul Nariman, N. (2016), "Influence of fluid-structure interaction on vortex induced vibration and lock-in phenomena in long span bridges", *Front Struct. Civ. Eng.*, **10**(4), 363-384. https://doi.org/10.1007/s11709-016-0353-y.

Bearman, P.W. (1984), "Vortex shedding from oscillating bluff Bodies", *Annu. Rev. Fluid Mech*., **16**, 195-222.

Bernitsas, M. M., Raghavan, K., Ben-Simon, Y. and Garcia, E.M.H. (2008), "VIVACE (vortex induced vibration aquatic clean energy): a new concept in generation of clean and renewable energy from fluid flow", *J. Offshore Mech. Arct.*, **130**(4), 041101-15. https://doi.org/10.1115/1.2957913.

Blevins, R.D. (1990), Flow-Induced Vibration, (2th Ed.), Van Nostrand Reinhold, New York.

Chaplin, J.R., Bearman, P.W., Huera Huarte, F.J. and Pattenden, R.J. (2005), "Laboratory measurements of vortex-induced vibrations of a vertical tension riser in a stepped current", *J. Fluid Struct*., **21**(1), 3-24. https://doi.org/10.1016/j.jfluidstructs.2005.04.010.

Chizfahm, A., Azadi Yazdi, E. and Eghtesad, M. (2018), "Dynamic modeling of vortex induced vibration wind turbines", *Renew Energ*, **121**(1), 632-643. https://doi.org/10.1016/j.renene.2018.01.038.

Dai, H.L, Yang, Y.W., Abdelkefi, A. and Wang, L. (2018), "Nonlinear analysis and characteristics of inductive galloping energy harvesters", *Commun. Nonlinear Sci. Numer. Simulat*, **59**(1), 580-591. https://doi.org/10.1016/j.cnsns.2017.12.009.

Dai, H.L., Abdelkefi, A. and Wang, L. (2014), "Piezoelectric energy harvesting from concurrent vortex-induced vibrations and base excitations", *Nonlinear Dynam*, **77**(3) 967-981. https://doi.org/10.1007/s11071-014-1355-8.

de Langre, E. (2006) , "Frequency lock-in is caused by coupled-mode flutter", *J. Fluid Struct.*, **22**(6-7), 783-791. https://doi.org/10.1016/j.jfluidstructs.2006.04.008.

Facchinetti, M.L., de Langre, E. and Biolley, F. (2004), "Coupling of structure and wake oscillators in vortex-induced vibrations", *J Fluid Struct.*, **19**(2), 123-140. https://doi.org/10.1016/j.jfluidstructs.2003.12.004,

Facchinetti, M.L., de Langre, E. and Biolley, F. (2004), "Vortex-induced travelling waves along a cable", *Eur. J. Mech. B-Fluid.*, **23**(1), 199-208. https://doi.org/10.1016/j.euromechflu.2003.04.004.

Farshidianfar, A. and Zanganeh, H. (2010), "A modified wake oscillator model for vortex-induced vibration of circular cylinders for a wide range of mass-damping ratio", *J. Fluid Struct*., **26**(3), 430-441. https://doi.org/10.1016/j.jfluidstructs.2009.11.005.

Gao, X., Xu, W., Bai, Y. and Zhu, H. (2018), "A novel wake oscillator model for vortex-induced vibrations prediction of a cylinder considering the influence of Reynolds number", *China Ocean Eng.*, **32**(2), 132-143. https://doi.org/10.1007/s13344-018-0015-z.

Griffin, O.M., Skop, R.A. and Koopmann, G.H. (1973), "The vortex-excited resonant vibrations of circular cylinders", *J Sound Vib*, **31**(2), 235-249. https://doi.org/10.1016/S0022-460X(73)80377-3.

Ji, C., Peng, Z., Mahbub Alam, M., Chen, W. and Xu, D. (2018), "Vortex-induced vibration of a long flexible cylinder in uniform cross-flow", *Wind Struct.*, **26**(5), 267-277. https://doi.org/10.12989/was.2018.26.5.267.

Jia, J., Shan, X., Upadrashta, D., Xie, T., Yang, Y. and Song, R. (2018), "Modeling and analysis of upright piezoelectric energy harvester under aerodynamic vortex-induced vibration", *Micromachines*, **9**(1), 667(19pp). https://doi.org/10.3390/mi9120667.

Keber, M. and Wiercigroch, M.A. (2007), "reduced order model for vortex–induced vibration of a vertical offshore riser in lock–in", *IUTAM Symposium on Fluid-Structure Interaction in Ocean*, Humburg, Germany.

Kurushina, V. and Pavlovskaia, E. (2017), "Wake oscillator equations in modeling vortex-induced vibrations at low mass ratios", OCEANS 2017, Aberdeen, UK.

Leblond, A. and Hardy, C. (2005), "Unifying calculation of vortex-induced vibrations of overhead conductors", *Wind Struct.* , **8**(2), 79-88. http://dx.doi.org/10.12989/was.2005.8.2.079.

Leclercq, T. and de Langre, E. (2018), "Vortex-induced vibrations of cylinders bent by the flow", *J. Fluid Struct.*, **80**(1), 77-93. https://doi.org/10.1016/j.jfluidstructs.2018.03.008.

Mathelin, L. and de Langre, E. (2005), "Vortex-induced vibrations and waves under shear flow with a wake oscillator model", *Eur. J. Mech. B-Fluid*., **24**(4), 478-490. https://doi.org/10.1016/j.euromechflu.2004.12.005.

Ogink, R.H.M. and Metrikine, A.V. (2010), "A wake oscillator with frequency dependent coupling for the modeling of vortex-induced vibration", *J. Sound Vib.*, **329**(26), 5452-5473. https://doi.org/10.1016/j.jsv.2010.07.008.

Postnikov, A., Pavlovskaia, E. and Wiercigroch, M. (2017), "2DOF CFD calibrated wake oscillator model to investigate vortex-induced vibrations", *Int. J. Mech. Sci*., **127**(1), 176-190. https://doi.org/10.1016/j.ijmecsci.2016.05.019.

Qu, Y. and Metrikine, A.V. (2016), "A wake oscillator model with nonlinear coupling for the VIV of rigid cylinder constrained to vibrate in the cross flow direction", *Proceedings of the 35th International Conference on Ocean, Offshore and Arctic Engineering*, Busan, South Korea.

Salvador, C.S., Teresa, J.A., Martinez, J.M., Bacasnot, M.C., Orilla, K.V., Cabana, R.J. and Ladaran, W.I. (2017), "design and construction of arc shaped and disc shaped pendulum for vortex bladeless wind generator", *Proceedings of the 25th International Conference on Systems Engineering*, Las Vegas, USA.

Skop, R.A. and Balasubramanian, S. (1997), "A new twist on an old model for vortex-excited vibrations", *J. Fluid Struct*., **11**(4), 395-412. https://doi.org/10.1006/jfls.1997.0085.

Skop, R.A. and Griffin, O.M. (1973), "A model for the vortex-excited resonant response of bluff cylinders", *J. Sound Vib*., **27**(2), 225-233.

Skop, R.A. and Luo, G. (2001), "An inverse-direct method for predicting the vortex-induced vibrations of cylinders in uniform and nonuniform flows", *J. Fluid Struct*., **15**(6), 867-884. https://doi.org/10.1006/jfls.2000.0381.

Song, R., Shan, X., Lv, F. and Xie, T. (2015), "A study of vortex-induced energy harvesting from water using PZT piezoelectric cantilever with cylindrical extension", *Ceram Int.*, **41**(1), 768-773. https://doi.org/10.1016/j.ceramint.2015.03.262.

Sun, Y., Li, M. and Liao, H. (2013), "Investigation on vortex-induced vibration of a suspension bridge using section and full

aeroelastic wind tunnel tests", *Wind Struct.*, **17**(6), 565-587. https://doi.org/10.12989/was.2013.17.6.565.

Vandiver, J.K., Jaiswal, V. and Jhingran, V. (2009), "Insights on vortex-induced, traveling waves on long risers", *J. Fluid Struct.*, **25**(4), 641-653. https://doi.org/10.1016/j.jfluidstructs.2008.11.005.

Violette, R., de Langre, E. and Szydlowski, J. (2007), "Computation of vortex-induced vibrations of long structures using a wake oscillator model: Comparison with DNS and experiments", *Comput. Struct.*, **85**(11-14), 1134-1141. https://doi.org/10.1016/j.compstruc.2006.08.005.

Wang, D., Chen, Y., Wiercigroch, M. and Cao, Q. (2016), "A three-degree-of-freedom model for vortex-induced vibrations of turbine blades", *Meccanica*, **51**(11), 2607-2628. https://doi.org/10.1007/s11012-016-0381-7.

Wang, D., Chen, Y., Wiercigroch, M. and Cao, Q. (2016), "Bifurcation and dynamic response analysis of rotating blade excited by upstream vortices", *Appl. Math. Mech.*, **37**(9), 1251-1274. https://doi.org/10.1007/s10483-016-2128-6.

Whitlock, R. (2015), *The Power of the Vortex: an Interview*, Renewable energy magazine, April.

Xu, W., Wu, Y., Zeng, X., Zhong, X. and Yu, J. (2010), "A new wake oscillator model for predicting vortex induced vibration of a circular cylinder", *J. Hydrodyn.*, **22**(3), 381-386. https://doi.org/10.1016/S1001-6058(09)60068-8.

Zhang, L.B., Dai, H.L., Abdelkefi, A. and Wang, L. (2019), "Experimental investigation of aerodynamic energy harvester with different interference cylinder cross-sections", *Energy*, **167**(15), 970-981. https://doi.org/10.1016/j.energy.2018.11.059.

FR